Thin film of coumarin-3-carboxylate and surfactant co-intercalated layered double hydroxide with polarized photoluminescence: a joint experimental and molecular dynamics study†

Dongpeng Yan,[a] Jun Lu,*[a] Jing Ma,[b] Min Wei,*[a] Shenghui Qin,[a] Li Chen,[a] David G. Evans[a] and Xue Duan[a]

Received 26th November 2009, Accepted 25th March 2010
First published as an Advance Article on the web 11th May 2010
DOI: 10.1039/b924821h

This paper describes a systematic investigation on the photophysical properties, thermal stability, and orientational structure of a coumarin-3-carboxylate (C3C) and dodecylsulfonate (DDS) co-intercalated Mg-Al-layered double hydroxide (C3C-DDS/LDH) system. C3C and DDS with different molar ratios were co-intercalated into the interlayer region of Mg-Al-LDH. The structures of the composites were characterized by X-ray diffraction (XRD), thermogravimetric and differential thermal analysis (TG-DTA). Fluorescence spectra demonstrate that the sample with 1.96% C3C molar percentage (with respect to the total organic components) exhibits the optimal luminous intensity. The fluorescence lifetime of C3C in C3C-DDS/LDH is enhanced significantly compared with that of pristine C3C solution (5.52 ns *vs.* 2.70 ns), revealing that the co-intercalation method is favorable for the improvement of the luminescence performances of the dye. C3C-DDS/LDH thin film was fabricated by the solvent evaporation method, which exhibits well polarized luminescence with the luminescent anisotropy of 0.10–0.15 at ambient temperature. Furthermore, molecular dynamics (MD) simulation was employed to calculate the basal spacing and molecular arrangement of intercalated C3C and DDS in the LDH matrix. The simulation results show that the intercalated C3C anions exhibit a tendency from tilted to vertical orientation relative to the inorganic layers as the interlayer DDS content increases. Moreover, the increase of the distance between C3C anions can be achieved enough upon the co-intercalation of DDS, presenting the key role of surfactant for preventing dye aggregation. Based on the combination of experimental and simulated studies, the photoluminescence properties of the C3C-DDS/LDH thin film were deeply studied and optimized, and a detailed understanding of the orientation of two individual guest molecules confined within the galleries of host layers was achieved.

1. Introduction

The organization of guest dye molecules into host matrixes has received much attention in recent years, for these solid materials may show desirably novel physical and chemical properties compared with their individual counterparts. They are considered as good candidates for solid state dye laser and luminescence materials.[1] Layered double hydroxides (LDHs) form one type of such solid host matrices, also known as "anion clay" compounds,[2,3] which can be described by the general formula $[M^{II}_{1-x}M^{III}_{x}(OH)_2]^{z+}A^{n-}_{z/n}\cdot yH_2O$, where M^{II} and M^{III} are divalent and trivalent metals respectively; A^{n-} is the anion to compensate for the positive charge of the hydroxide layers. Based on the attractive intercalation feature, LDHs have been applied in the areas of catalysis,[4] separation process,[5] and the storage and delivery of biological molecules.[6] Recently, many luminescent dye molecules,[7] such as perylene,[7a] pyrene chromophores,[7b] and rhodamine B,[7c] incorporated in LDHs systems were also investigated, for the immobilized dye molecules may exhibit novel photophysical behavior in a confined and stable microenvironment, which is absent in solution and also favorable for their application as luminescent materials. Furthermore, the host–guest interaction based on the electrostatic, H-bond and van der Waals interaction can facilitate a homogeneous distribution of the dye molecules in the galleries of LDH at the molecular level. Last but not least, the LDH matrix provides a higher mechanical and thermal stability for the dye molecules as well as reduces the environmental pollution and operational risk, which meets the fabrication need of solid state light-emission materials.

However, relative poor luminescence properties (including fluorescence red-shift, broadening, and even quenching) still can be found in many dye intercalated LDH systems. These phenomena can be attributed to the formation of dye aggregates in the LDH galleries due to the π–π or dipole–dipole interaction, which is detrimental for the optical applications of dye/LDH systems. For instance, it was reported that composites of perylene derivative-intercalated Zn-Al-LDH show complete fluorescence quenching.[7a] Accordingly, it is of great importance to

[a]*State Key Laboratory of Chemical Resource Engineering, Beijing University of Chemical Technology, Beijing, 100029, P. R. China. E-mail: lujun@mail.buct.edu.cn; weimin@mail.buct.edu.cn; Fax: +86-10-64425385; Tel: +86-1064412131*
[b]*School of chemistry and chemical engineering, Key Laboratory of Mesoscopic Chemistry of MOE, Nanjing University, Nanjing, 210093, P.R. China*

† Electronic supplementary information (ESI) available: TG-DTA curves of C3C and C3C intercalated LDH; elemental composition for the C3C-DDS/LDH; fluorescence decay of C3C-DDS/LDH and C3C solution; schemes for Fig. 7, 10, 11, 12. See DOI: 10.1039/b924821h

effectively avoid the formation of dye aggregates in the galleries of LDH for the enhancement of the fluorescence efficiency. One effective solution to the dye aggregation is the introduction of a surfactant into LDH galleries as a second guest, although the detailed effect of surfactant is still not fully understood.

In recent years, due to the limitation of the experimental characterizations, much attention has been focused on computer simulations for investigating materials at the atomic/molecular scale in the field of chemistry. These theoretical simulations provide an effective and complementary method to study and predict the structures and properties of new types of functional materials. Molecular dynamics (MD) is such a technique based on Newton's second law, which can be used to simulate the real movement of atomic systems. Correspondingly, MD is employed to simulate the LDH-based anionic clay materials and to probe many thermodynamic properties of the guest molecules in the confined environment of LDH layers, such as radial distribution functions (RDFs) and the self-diffusion properties. Moreover, the detailed orientational arrangement of anions within the LDH galleries, such as citrate,[8a] diclofenac drug,[8b] and nitrate anions,[8c] were also studied, since this information is not easily available by the current experimental observations. To the best of our knowledge, most MD simulation studies were mainly concerned about the single guest anion in the LDH galleries, and very few studies reported two or more anionic species co-intercalated into LDH systems.[8d] Therefore, it is necessary to develop and investigate the co-intercalated LDH systems to meet the needs of the integration of the multi-functional guest anions into the LDH layer.

Coumarin is one of the important laser dyes with high luminescent quantum yield, which is extensively used in the fields of photoluminescent and electroluminescent materials. In the present work, the co-intercalation of coumarin-3-carboxylate (C3C) and dodecylsulfonate (DDS) with different molar ratios in the galleries of LDH was performed, to study their structure, thermal stability and the detailed fluorescence properties of these inorganic–organic intercalation compounds. The coexistence of DDS plays an important role for preventing the aggregation of C3C and providing a homogeneous and nonpolar environment to enhance its luminescent performance. The maximal luminescence intensity and fluorescence lifetime were firstly obtained by exploring the correlation between C3C luminescence and its concentration in the LDH galleries. Meanwhile, the C3C-DDS/LDH thin films were prepared by the solvent evaporation method, which exhibit well-defined polarized photoemission anisotropy. Furthermore, MD simulation based on a modified cff91 forcefield[8e,f] was employed to analyze the basal spacing and orientations of the confined C3C and DDS anions within the LDH matrix. The simulation results are in reasonable agreement with the experimental ones, demonstrating the feasibility of MD simulation for this dye/LDH system. Therefore, this work not only confirms that the co-intercalation method is favorable for the enhancement of luminescence efficiency of solid-state fluorescence materials, but also provides a detailed understanding of the structure and preferred arrangement of two different guest species confined between the sheets of LDHs. It is expected that C3C intercalated LDH films can be potentially applied in the field of solid state polarized luminescent materials.

2. Experimental

Materials

Sodium coumarin-3-carboxylate (C3C) and the surfactant, sodium dodecylsulfonate (DDS, >95%), were purchased from Sigma Chemical. Co. Ltd. NaOH, $Mg(NO_3)_2 \cdot 6H_2O$ and $Al(NO_3)_3 \cdot 9H_2O$ were purchased from Beijing Chemical Corporation Limited and used without further purified.

Precursor solutions

Solution A: $Mg(NO_3)_2 \cdot 6H_2O$ (0.002 mol) and $Al(NO_3)_3 \cdot 9H_2O$ (0.001 mol) dissolved in 70 mL of deionized water. Solution B: NaOH (0.006 + b mol), DDS (a mol) and C3C (b mol, in which $a + b = 0.001$ mol; $a : b = 100 : 0$; 100 : 1; 100 : 2; 100 : 5; 100 : 10; 100 : 20; 3 : 1; 1 : 1; 1 : 3; 0 : 100. $x\% = b/(a+b)$) dissolved in 70 mL of mixture solvent of deionized water and anhydrous ethanol (1 : 1, v/v).

Synthesis of DDS-C3C/LDH powder and thin film

Solution A (70 mL) and solution B (70 mL) were simultaneously added to a colloid mill and mixed for 1 min (rotating at 3000 rpm). It is anticipated that the two guest species formed directly and simultaneously in the galleries of LDH during the coprecipitation process. The resulting slurry was removed from the colloid mill and sealed into a Teflon-lined stainless steel autoclave, purged with nitrogen atmosphere and heated at 100 °C for 1 day. The product was washed with hot distilled water and anhydrous ethanol several times until the filtrate was colorless, and then dried in a vacuum oven at 60 °C for 6 h. The film of C3C-DDS/LDH was prepared by the solvent evaporation method: a suspension of C3C-DDS/LDH in ethanol (1 mg/mL) was ultrasonically dispersed and then spread on a quartz substrate which was previously cleaned thoroughly by an ultrasonic anhydrous ethanol bath.

Characterization

Powder XRD patterns of the samples were recorded using a Rigaku XRD-6000 diffractometer under the following conditions: 40 kV, 30 mA, Cu Kα radiation. The powder samples were step-scanned in steps of 0.04° (2θ) in the range from 2 to 70° using a count time of 10 s/step. The morphology of the C3C-DDS/LDH thin film was investigated by using a scanning electron microscope (SEM Hitachi S-3500) equipped with an EDX attachment (EDX Oxford Instrument Isis 300), and the accelerating voltage applied was 20 kV. The surface roughness data were obtained by using the atomic force microscopy (AFM) software (Digital Instruments, Version 6.12). Thermogravimetric analysis and differential thermal analysis (TG-DTA) were carried out on a PCT-1A thermal analysis system under ambient atmosphere with a heating rate of 10 °C/min. Content analysis of metals was performed by ICP atomic emission spectroscopy on a Shimadzu ICPS-7500 instrument using the solutions prepared by dissolving the samples in dilute nitric acid. Carbon, hydrogen, and nitrogen analyses were carried out using a Perkin-Elmer Elementarvario elemental analysis instrument. The solid state fluorescence spectra of powders were recorded on a RF-5301PC

fluorospectrophotometer under identical conditions with excitation wavelength of 360 nm and emission spectra in the range 400–600 nm. The width of both the excitation and emission slit is 3 nm. Steady-state polarized photoluminescence measurements were recorded with an Edinburgh Instruments' FLS 920 fluorimeter. The emission spectra and fluorescence lifetime were measured by exciting at 360 nm with a 450 W Xe arc lamp, and the percentage contribution of each lifetime component to the total decay was calculated with the F900 Edinburgh instruments software. The solid state UV-vis adsorption spectra were collected in the range from 210 to 800 nm on a Shimadzu U-3000 spectrophotometer. The width of the slit is 1.0 nm, and $BaSO_4$ was used as reference.

3. Theoretical calculation

Firstly, an ideal LDH layer model with tetragonal superlattice of the $R\bar{3}m$ space group was constructed according to our previous work,[8e,f] for reducing the computational complexity without affecting the precision. The supercell containing 32 Mg atoms and 16 Al atoms was built based on the following rule: each [AlO_6] octahedron is surrounded by six [MgO_6] octahedra, and each [MgO_6] octahedron is, in turn, surrounded by three [AlO_6] octahedra, ensuring that Al atoms will not occupy adjacent octahedra. Therefore, every supercell of the octahedral layer has 48 metal atoms and 96 OH groups under the condition of $\alpha = \beta = 90°$, and the distance between adjacent metal atoms is 3.05 Å. Therefore, a supercell was constructed, with lattice parameters $a = 21.13$ Å, $b = 18.30$ Å, $c = 24$ Å (experimental result), $\alpha = \beta = \gamma = 90°$. The supercell was treated as P1 symmetry and all of the lattice parameters were considered as independent variables in the simulation. A 3-dimensional periodic boundary condition was applied in the system, and the simulated supercell can be repeated infinitely in three directions. C3C (Fig. 1b) and DDS anions (Fig. 1c) were introduced into the simulated supercell with different ratios (C3C : DDS = 0 : 16; 4 : 12; 8 : 8; 12 : 4; 16 : 0) as the initial configurations. Furthermore, 40 water molecules (the experimental hydration conditions determined by TG-DTA) were located randomly in the supercell based on the assumption that these molecules occupy the whole available interlayer space as much as possible. As a result, the formula of the simulated structure can be expressed as: $Mg_{32}Al_{16}(OH)_{96}(C_{10}H_5O_4)_x(C_{12}H_{25}SO_3)_{16-x}\cdot 40H_2O$ ($x = 0, 4, 8, 12, 16$).

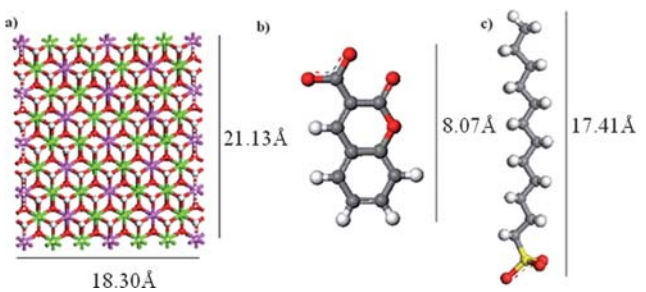

Fig. 1 a) The tetragonal superlattice model for Mg-Al-LDH layer (color code: white: H; red: O; pink: Al; green: Mg), b) structural model of coumarin-3-carboxylate (C3C, $C_{10}H_5O_4^-$), and c) structural model of dodecylsulfonate (DDS, $C_{12}H_{25}SO_3^-$).

A modified cff91 forcefield was employed to perform MD simulation in the whole process. The Charge Equilibration (QEq) method[9] was used to calculate atomic charges of the layer, in which the partial charges are +0.703e for Mg, +1.363e for Al, −0.537e for O and +0.243e for H. Other forcefield parameters for the anions and water molecules were referred to the cff91 forcefield.[10] The NBO analysis[11] was employed to calculate the partial charges of C3C and DDS anions on the B3LYP/6-31G** level using the Gaussian 03 programs.[12] For water molecule, the partial charges came from the simple point charge (SPC) water model.[13] In potential energy calculations, the long range coulomb interactions between partial charges were computed by the Ewald summation technique[14] and a "spline cutoff" method was used to calculate van der Waals interaction. After energy minimization was applied on the initial model, MD simulations were performed in isothermal-isobaric (NPT) ensemble with the temperature of 300 K and the pressure of 0.1 MPa (about 1 atm). The Andersen method[15] and Berendsen method[16] were used to control temperature and pressure, respectively. The total simulation time was 300 ps with the simulation time step of 1 fs. The result shows that the system reached equilibrium with lattice parameters and total potential energy fluctuating around a constant value within the first 50 ps, so the dynamic trajectories were recorded every 20 fs in the remaining 250 ps in order to analyze the ensemble average values. All the simulations were performed using the Discover module in the Material Studio software package.[17]

4. Results and discussion

4.1. Characterization of the C3C-DDS/LDH powder samples

A. Crystal structure and thermal stability. The XRD patterns of C3C and DDS co-intercalated LDH samples C3C-DDS/LDH (x%) are displayed in Fig. 2A, where x% stands for the initial molar percentage of C3C within the summation of C3C and DDS. The patterns of these samples can be indexed to a trigonal lattice with R-3m rhombohedral symmetry. The basal spacing can be calculated from averaging the positions of the three harmonics: $c = 1/3\,(d_{003} + 2d_{006} + 3d_{009})$. It can be observed from Fig. 2B that the basal spacing of C3C-DDS/LDH increases slightly at first from 2.421 nm (x% = 0%) to the maximum (2.453 nm, x% = 0.99%), and then decreases gradually to the minimum of 1.752 nm (x% = 100%), upon increasing the C3C component. The variation of the interlayer spacing can be attributed to the different arrangements of interlayer guest species with different ratios of DDS and C3C, which will be further investigated in the molecular dynamics section. Moreover, the basal spacing does not change obviously for the samples of C3C-DDS/LDH (x% = 0%–25%), suggesting the DDS content imposes more influence on the basal spacing compared with C3C anions. The basal spacing for the C3C/LDH composite is close to the reported one (1.79 nm) prepared by the calcination/reconstruction method.[7d] To investigate the thermolysis behavior of both pristine and totally intercalated C3C within the LDH galleries, thermogravimetric and differential thermal analysis (TG-DTA) were performed for these two samples. TG-DTA curves (see supplementary information (ESI†): Fig. S1) show that the sharp weight loss of C3C with an exothermic peak appears at 441 °C,

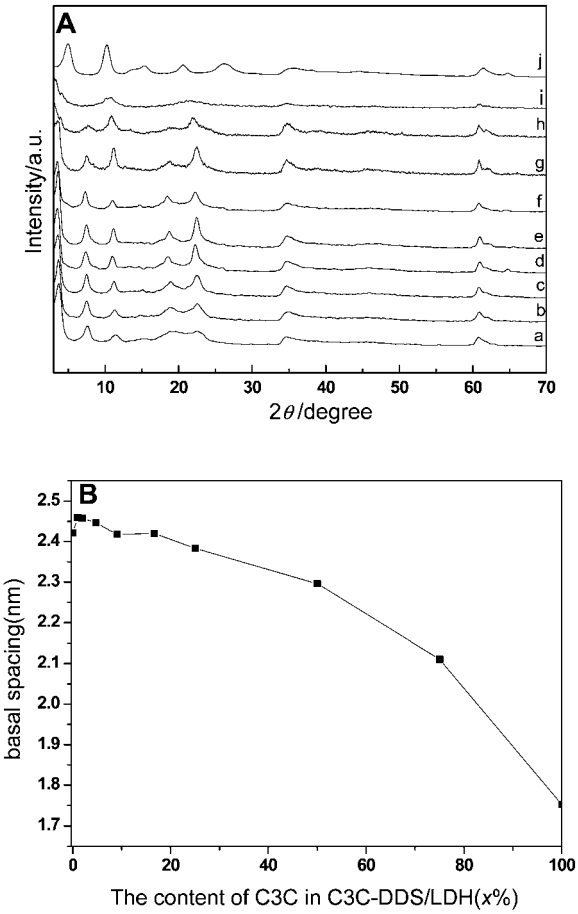

Fig. 2 (A) Powder XRD patterns of C3C-DDS/LDH (x%) (a. 0%, b. 0.99%, c. 1.96%, d. 4.76%, e. 9.09%, f. 16.67%, g. 25.0%, h. 50.0%, i. 75.0%, j. 100%). (B) The plot of basal spacings *vs.* C3C concentration.

whereas the weight loss of C3C/LDH with a sharp exothermic peak occurs at 468 °C, indicating that the thermal stability of C3C molecule is enhanced when intercalated into the galleries of LDHs. Moreover, based on the TG-DTA curve of C3C/LDH, the interlayer water content can be estimated as *ca.* 10.8% of the total weight, with the assumption that the interlayer water molecules totally disappear before 190 °C. The results of elemental analysis show that the experimental ratio of C3C to DDS in the C3C-DDS/LDH systems is close to the nominal ratio (ESI:† Table S1).

B. Optimal luminous intensity and fluorescence lifetime. The fluorescence emission spectra for C3C-DDS/LDH samples with different molar ratios of C3C to DDS are shown in Fig. 3. The fluorescence intensity increases at first (x% = 0.99%) to a maximum, and then decreases with the increase of the C3C content (shown in the inset plot). The optimal luminous intensity presents in the sample with x% = 1.96%, and the emission peak appears at 471 nm with the full width at half maximum (FWHM) of *ca.* 45 nm, which corresponds to the S_1–S_0 transition (the transition dipole moment along the long axis direction of C3C). The maximum emission wavelength shifts to 490 nm (consistent with the previous report[7d]) and its intensity falls quickly when the C3C content increases to 100%. This phenomenon can be

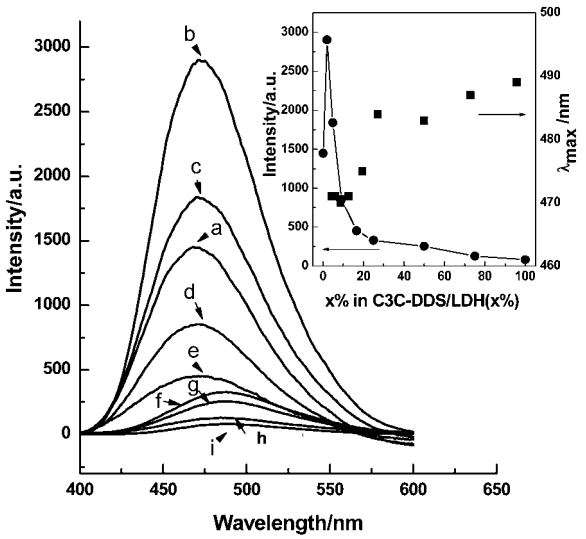

Fig. 3 The photoemission spectra of the C3C-DDS/LDH samples with the excitation wavelength of 360 nm. The inset plot shows the fluorescence intensity and the maximum emission wavelength varying with the increase of C3C content in the C3C-DDS/LDH (x%): (a) 0.99%, (b) 1.96%, (c) 4.76%, (d) 9.09%, (e) 16.67%, (f) 25.0%, (g) 50.0%, (h) 75.0%, (i) 100%.

attributed to the following reason: the C3C anions exhibit single molecular luminescence with low C3C content in the LDH matrix, accounting for the increase in the luminous intensity firstly; the formation of dye aggregation occurs with further increase in C3C content, resulting in the weak fluorescence intensity and the red shift of emission spectra.

The solid state UV-vis absorption spectra of the C3C-DDS/LDH(x%) samples are shown in Fig. 4. The maximum of absorption bands located around 290 and 360 nm increases upon increasing the concentration of C3C. Furthermore, an absorption shoulder band at ~400 nm appears when the content of C3C increases to 16.7%, and the spectra become broad. This can be assigned to the appearance of J-type aggregation of C3C in the

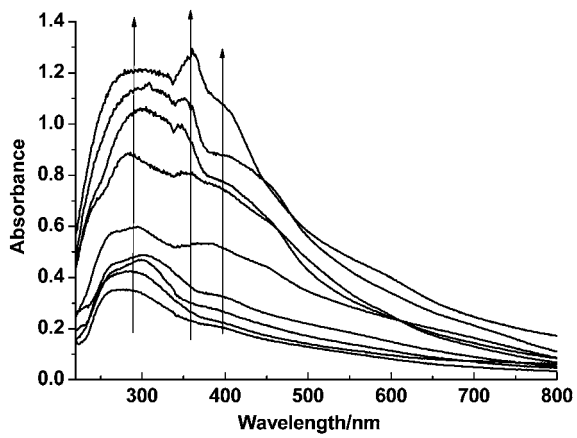

Fig. 4 The UV-vis absorption spectra of the C3C-DDS/LDH samples varying with the increase of C3C content in the C3C-DDS/LDH (x%, from bottom to top: 0.99%, 1.96%, 4.76%, 9.09%, 16.67%, 25.0%, 50.0%, 75.0%, and 100%).

galleries of LDH, which is consistent with the red-shift phenomenon in the fluorescence emission spectra discussed above. Compared with the pristine C3C intercalated LDH system, the C3C aggregation cannot form in the samples with low C3C content, by which the improvement of luminous efficiency can be achieved. It was reported that surfactants or organic solvents can alter the aggregation of photoactive species,[18] and the presence of the long-chain surfactant led to a high emission intensity in the system of oxazine dye intercalated cation clay.[19] In our opinion, the intercalated long-chain surfactant molecules achieved a homogeneously hydrophobic interlayer environment, which can isolate dye anions and thus prevent the fluorescence self-quenching.

The samples of C3C-DDS/LDH(x%) were studied by detecting their fluorescence decays, with the excitation and emission wavelengths of 360 and 475 nm, respectively. The fluorescence lifetimes were obtained by fitting the decay profiles (as shown in Fig. S2 in ESI†) with one-exponential and double-exponential forms respectively, and the results are tabulated in Table 1. In the double-exponential case, the average lifetime, $<\tau>$, is also listed.

Compared with the aqueous solution of C3C (1×10^{-5} M, *ca.* 2.70 ns), the single-exponential fluorescence lifetime of C3C-DDS/LDH (x%) increases remarkably at first from 3.07 ns ($x =$ 0.99%) to the maximum (5.52 ns, $x = 1.96$%), and then decreases gradually to the minimum (3.52 ns, $x = 16.67$%). All the fluorescence lifetimes of these solid samples are longer than that of the aqueous solution, demonstrating that the nonradiative relaxation of C3C molecules in excited states could be effectively suppressed when located between the rigid LDH layers. Moreover, the longest fluorescence lifetime obtained by both one-exponential and double-exponential fitting is found for the sample of C3C-DDS/LDH (1.96%), in accordance with that of the optimal luminous intensity above. The two fluorescence lifetimes can be attributed to different dye states in the LDH matrix. The long lifetime possibly corresponds to the intercalated C3C in the galleries of LDH and the short one is attributed to the adsorbed C3C on the surface of LDH particles, since the intercalated C3C molecules are more stably immobilized.

Table 1 Fluorescence decay data of the powder samples of C3C-DDS/LDH (x%)[a]

x (%)	n	τ_i(ns)	A_i(%)	$<\tau>$(ns)	χ^2
0.99	1	3.07	100.00		10.475
	2	7.43	58.52	4.91	1.233
		1.36	41.48		
1.96	1	5.52	100.00		2.517
	2	6.79	75.51	5.74	1.102
		2.52	24.49		
4.76	1	4.74	100.00		6.368
	2	7.08	65.39	5.32	1.289
		2.00	34.61		
9.09	1	4.42	100.00		9.648
	2	7.78	66.24	5.64	1.131
		1.45	33.76		
16.67	1	3.52	100.00		10.725
	2	6.99	51.54	4.27	1.552
		1.37	48.46		

[a] τ_i is the fluorescence lifetime; A_i stands for the percentage of τ_i. The goodness of fit is indicated by the value of χ^2. In the double-exponential case, $<\tau> = A_1\tau_1 + A_2\tau_2$; $A_1 + A_2 = 1$.

4.2 The characterization of C3C-DDS/LDH thin films

A. The orientation and morphology. In this section, our attention was mainly focused on the sample with C3C content of 1.96%, due to its better photoemission behavior and longer fluorescence lifetime. As shown in Fig. 5, the strong basal reflections (00l) and the absence of any non-basal reflections (h, $k \neq 0$) for the thin films of C3C-DDS/LDH (1.96%) are as expected owning to the extremely well c-oriented assembly of LDH platelets. Moreover, this can be further confirmed by the SEM image (Fig. 6a) that the LDH lamellar crystallites are stacked with ab-plane parallel to the substrate. The thin film is continuous and uniform, with the average film thickness of *ca.* 1.2 μm (Fig. 6b). As a result, it can be anticipated that the thin film may exhibit anisotropic light-emitting properties. Fig. 6c shows the macroscopic photograph of the colorless and transparent C3C-DDS/LDH thin film (2 cm × 2 cm), and well-defined and uniform blue fluorescence was observed under UV radiation (365 nm) as shown in Fig. 6d. The AFM topographical image

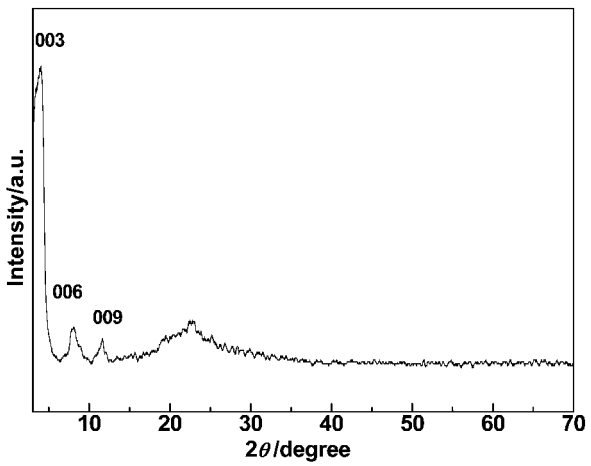

Fig. 5 XRD pattern of the C3C-DDS/LDH (1.96%) thin film.

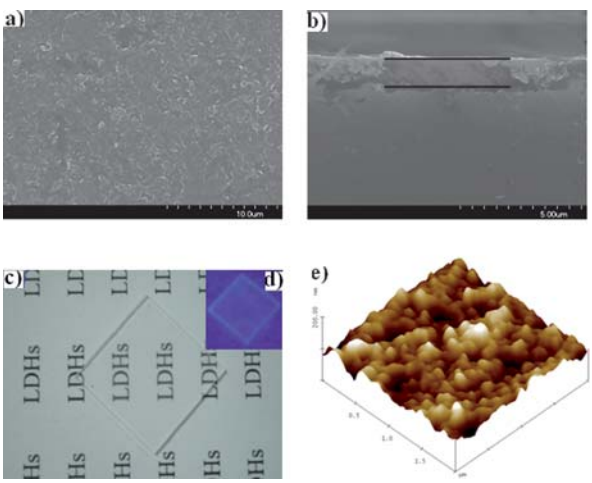

Fig. 6 a, b) Top view and side view of SEM images of the C3C-DDS/LDH (1.96%) thin film; c, d) the photographs of the thin film on quartz substrates under daylight and UV radiation (365 nm); e) tapping-mode AFM image of the thin film.

(2 μm × 2 μm) of the thin film is illustrated in Fig. 6e, and the average root-mean-square (rms) roughness of the film is *ca.* 8.60 nm, indicating the surface of the thin film is relative smooth.

B. Fluorescence lifetime and polarized fluorescence of the thin films. The fluorescence lifetimes of the C3C-DDS/LDH thin films ($x\% = 0.99\%$, 1.96%, and 4.76%) were further measured under the same conditions as the powder samples mentioned above. As shown in Table 2, fluorescence lifetimes of the thin films are nearly the same as those of the powder samples, confirming that the fluorescence properties remain unchanged during the preparation of thin films. Meanwhile, the C3C-DDS/LDH (1.96%) thin film possesses both the longest fluorescence lifetime and the average lifetime, consistent with that of the powder samples.

To further investigate the fluorescence polarization properties of the as-prepared C3C-DDS/LDH thin film, the anisotropic value r was measured.[20] r can be expressed as the formula:

$$r = \frac{I_{VV} - GI_{VH}}{I_{VV} + 2GI_{VH}} \quad (1)$$

where $G = I_{HV}/I_{HH}$, determined from the C3C aqueous solution; I_{VH} stands for the PL intensity obtained with vertical polarized light excitation and horizontal polarization detection, and I_{VV}, I_{HH}, I_{HV} are defined in a similar way. Theoretically, the value of r is in the range from −0.2 (absorption and emission transition dipoles are perpendicular to one another) to 0.4 (two transition dipoles are parallel to each other). The polarized photoemission spectra of the C3C-DDS/LDH (1.96%) thin film are displayed in Fig. 7. Two typical measurement setups of polarized fluorescence (the incident excitation light run along the glancing and normal direction of the thin film as shown in Scheme S1 in ESI†) were employed to determine the fluorescence anisotropic value r. It was observed that the C3C-DDS/LDH (1.96%) thin film shows well-defined blue fluorescence anisotropy between the parallel and perpendicular to the excitation polarized direction (I_{VV} *vs.* I_{VH}). The anisotropic value (r) is *ca.* 0.15 for horizontal excitation (Fig. 7a) and *ca.* 0.10 for vertical excitation (Fig. 7b), demonstrating the uniform dispersion and well-oriented C3C anions in the galleries of LDH. Moreover, the uniform r value ranging in 450–600 nm indicates that polarization scrambling *via* π–π interaction is minimal in the thin film.

Table 2 Fluorescence decay data of the C3C-DDS/LDH(x%) films[a]

x (%)	n	τ_i (ns)	A_i (%)	<τ> (ns)	χ^2
0.99	1	2.70	100.00		12.65
	2	8.80	43.84	4.73	1.367
		1.56	56.16		
1.96	1	5.03	100.00		3.39
	2	8.76	43.36	5.82	1.187
		3.52	56.64		
4.76	1	4.83	100.00		3.34
	2	8.23	50.86	5.66	1.083
		3.01	49.14		

[a] The meanings of τ_i, A_i, χ^2, <τ> are the same as described in Table 1.

4.3. Molecular dynamics simulation

A. The basal spacing and arrangement of C3C in the galleries of LDH. The basal spacing for five typical models of (C3C-DDS/LDH, $x\% = 0\%$, 25%, 50%, 75%, 100%) were calculated for further comparison with the experimental results. It can be seen from Fig. 8 that the simulated basal spacings are systematically very close to the experimental values with the average error of 0.074 nm, confirming the feasibility of MD simulation for this C3C and DDS co-intercalated LDH system. The typical snapshots of these configurations are shown in Fig. 9, which can help to further understand the structure and orientation of C3C and

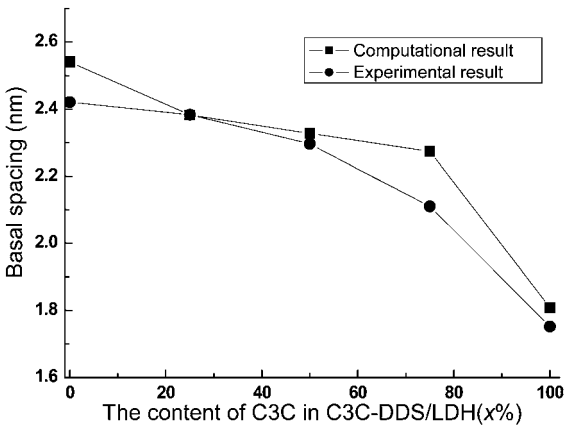

Fig. 8 The computational and experimental basal spacings as a function of the C3C content for the samples of C3C-DDS/LDH (0%, 25%, 50%, 75%, 100%).

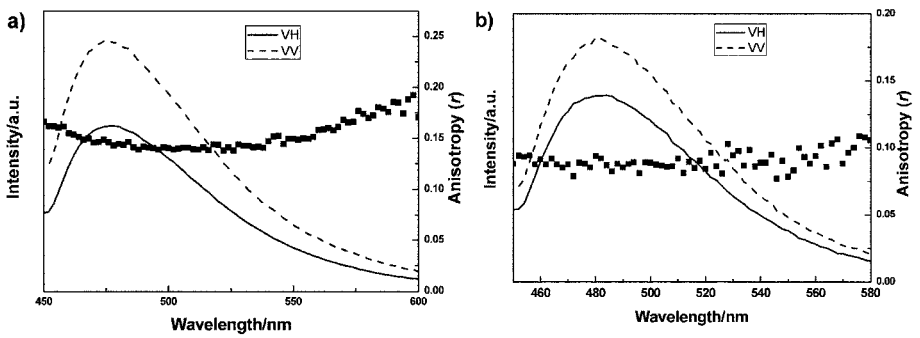

Fig. 7 Polarized fluorescence profiles in the VV, VH modes and anisotropic value (r) for the C3C-DDS/LDH (1.96%) thin film sample. a) and b) correspond to excitation light with glancing and normal incidence geometry respectively, as shown in Scheme S1 in ESI.†

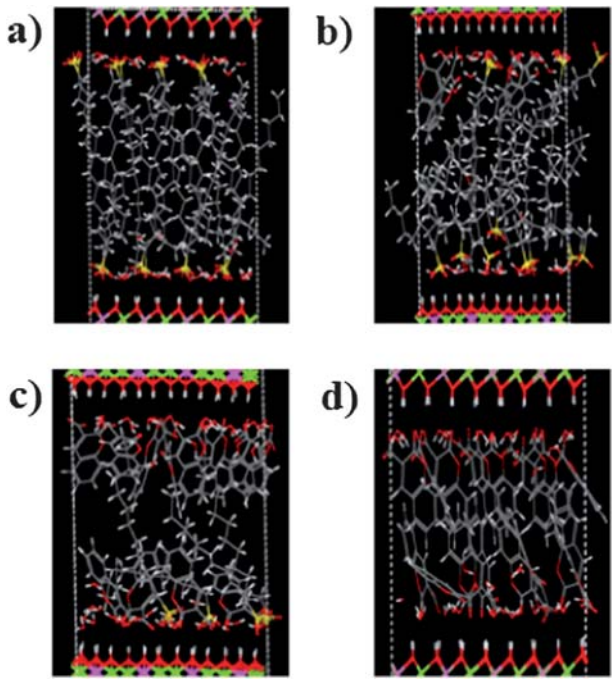

Fig. 9 Snapshots of the simulated equilibrium structures for C3C-DDS/LDH (x%): a) 0%, b) 25%, c) 75%, d) 100%.

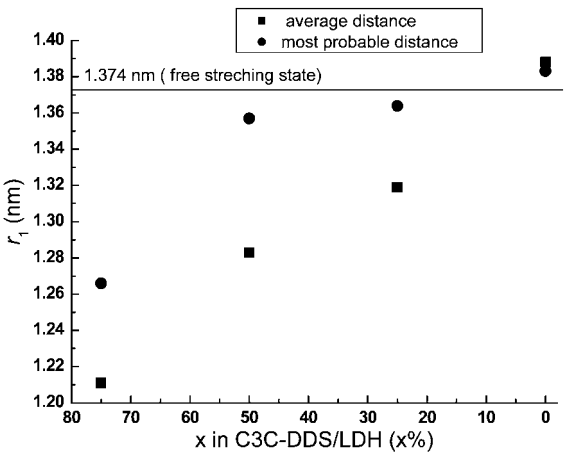

Fig. 10 The distance r_1 between C1 and C12 (the terminal C atoms) in DDS for the samples of C3C-DDS/LDH (0%, 25%, 50%, 75%).

DDS in the galleries of LDH. To investigate the variation of the basal spacing influenced by the ratio of C3C/DDS, the flexibility of the DDS anions was studied based on calculating the distance r_1 between C1 and C12 (the terminal C atoms, see Scheme S2 in ESI†) in DDS. Fig. 10 shows the dependence of r_1 on the DDS content, from which it can be found that the average and most probable value of r_1 increases upon increasing DDS content, and the average r_1 under different states is systematically lower than that of the stretching state of free DDS anion (1.374 nm). This suggests that the DDS anions exhibit twisting and stretching state under low and high DDS content, respectively (Scheme S2 in ESI†). This may give rise to the decreased basal spacing upon decreasing DDS content, just as XRD observations.

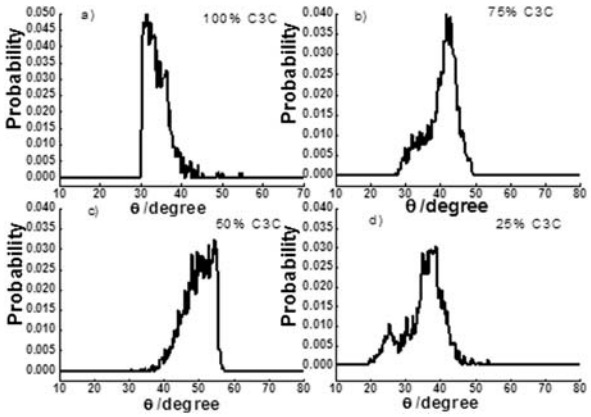

Fig. 11 The distributions of orientational angle θ (the plane of C3C with respect to the LDH layer) with different ratios of C3C to DDS for C3C-DDS/LDH (x%): a) 100%, b) 75%, c) 50%, d) 25%.

The orientation of the C3C anions in the LDH galleries is an important parameter to understand the properties of C3C anions in a confined environment. Angle θ stands for the orientational angle of the C3C plane with respect to the LDH layer (Scheme S3 in ESI†). Fig. 11 shows the distribution of θ with different ratios of C3C to DDS (C3C-DDS/LDH, $x\% = 100\%$, 75%, 50%, 25%). The orientational angle varies between 29 and 55° with the most probable angle of *ca.* 32° for the pristine C3C intercalated LDH system. It can be also observed from Fig. 9d that all the C3C molecules are inclining to the layers, attributed to the strong electrostatic interaction between the positive-charged host layers and the C3C anions. When the ratio of DDS to C3C is 1 : 3, the distribution of θ is mainly populated from 27 to 50° with the optimal angle of 42°. As the molar ratio of DDS/C3C increases to 1 : 1, the angle distribution from 35 to 58° is observed, and it exhibits nearly normal distribution with the maximum likelihood angle of 54°. For the C3C-DDS/LDH (25%) sample, the distribution of θ angle becomes narrow and the optimal angle is 39°. It thus can be concluded from Fig. 11 that the guest molecules have a tendency to change from a tilted to a vertical arrangement with respect to the layers as the DDS/C3C ratio increases from 0 to 1 : 1, due to the enlargement of the basal spacing upon increasing DDS content. The distribution of θ angle for the C3C-DDS/LDH (25%) with high DDS content corresponds to the relative rigid environment imposed by the DDS which restricts the flexible space for the C3C guest anions.

B. The distance between C3C anions. It is known that the introduction of long-chain surfactant anions can isolate the dye anions and prevent the formation of aggregates. However, detailed isolation effect of surfactant has not been further investigated. The distance between the two nearest C3C anions in the LDH galleries (r_2) was defined as the distance between centers of the two bridge C atoms (C2 and C3, Scheme S4 in ESI†) in C3C anions. Fig. 12 shows the average distance between two nearest C3C anions $\langle r_2 \rangle$ with different C3C/DDS ratios. Compared with the C3C/LDH ($x\% = 100\%$), the $\langle r_2 \rangle$ increase by *ca.* 26%, 44%, 61% for the C3C : DDS ratios of 3 : 1, 1 : 1, 1 : 3, respectively. The results further demonstrate that the DDS can enlarge the distance between dye molecules effectively, dilute and

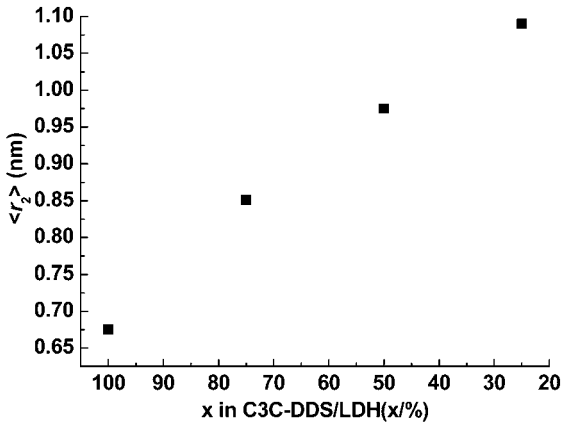

Fig. 12 Average distance $<r_2>$ between the two nearest C3C anions for C3C-DDS/LDH (x = 25%, 50%, 75%, 100%).

isolate the interlayer C3C molecules. This is consistent with the experimental observation described above.

Conclusions

In summary, the photoluminescence properties of C3C and DDS co-intercalated Mg-Al-LDH for both powder and thin film samples have been investigated. TG-DTA indicates that the thermal stability of C3C is enhanced upon intercalation. The optimal luminous intensity and fluorescence lifetime were achieved for the C3C-DDS/LDH with the C3C molar percentage of 1.96%. Compared with the C3C aqueous solution, the fluorescence lifetime of C3C-DDS/LDH (x% = 0.99–16.67%) composites increases greatly, demonstrating that the immobilization of C3C anions between the rigid LDH galleries can suppress the nonradiative relaxation process effectively. Moreover, the C3C-DDS/LDH (1.96%) thin films were prepared by the solvent evaporation method with well *c*-oriented morphology. The thin film shows well-defined polarized luminescence with the fluorescence anisotropy of 0.10–0.15. Molecular dynamics simulation was employed to study the dye arrangement of the C3C-DDS/Mg-Al-LDH system. The basal spacing with different C3C/DDS ratios was investigated, and the results are comparable with the experimental ones. C3C anions exhibit a tendency to change from a tilted to a vertical arrangement with respect to the LDH layers with increasing DDS content. The isolation effect for dye anions induced by DDS is also discussed. The DDS anions exhibit twisting and stretching states under low and high interlayer contents, and the distance between two C3C anions can be enlarged upon co-intercalation with DDS, which present a quantitative explanation for the key role of DDS for preventing dye aggregation. Therefore, by virtue of combination of experimental technique and theoretical calculation, this work not only reports a detailed investigation on the photophysical properties and thermolysis of dye molecules confined in the LDH matrix, but also provides a further understanding of the orientation of dye in the galleries of LDH.

Acknowledgements

This work was supported by the National Natural Science Foundation of China, the 111 Project (Grant No.: B07004), the 973 Program (Grant No.:2009CB939802) and the Chinese Universities Scientific Fund (Grant No.: ZZ0908).

Notes and references

1 C. M. Carbonaro, A. Anedda, S. Grandi and A. J. Magistris, *J. Phys. Chem. B*, 2006, **110**, 12932.
2 (*a*) A. M. Fogg, V. M. Green, H. G. Harvey and D. O'Hare, *Adv. Mater.*, 1999, **11**, 1466; (*b*) A. I. Khan and D. O'Hare, *J. Mater. Chem.*, 2002, **12**, 3191.
3 (*a*) F. Leroux and C. Taviot-Guého, *J. Mater. Chem.*, 2005, **15**, 3628; (*b*) D. Yan, J. Lu, M. Wei, J. B. Han, J. Ma, F. Li, D. G. Evans and X. Duan, *Angew. Chem., Int. Ed.*, 2009, **48**, 3073; (*c*) D. Yan, J. Lu, M. Wei, J. B. J. Ma, D. G. Evans and X. Duan, *Chem. Commun.*, 2009, 6358.
4 B. Sels, D. De Vos, M. Buntinx, F. Pierard, K. D. Mesmaeker and P. Jacobs, *Nature*, 1999, **400**, 855.
5 A. M. Fogg, J. S. Dunn, S. G. Shyu, D. R. Cary and D. O'Hare, *Chem. Mater.*, 1998, **10**, 351.
6 Q. Yuan, M. Wei, D. G. Evans and X. Duan, *J. Phys. Chem. B*, 2004, **108**, 12381.
7 (*a*) J. Bauer, P. Behrens, M. Speckbacher and H. Langhals, *Adv. Funct. Mater.*, 2003, **13**, 241; (*b*) S. Gago, T. Costa, J. S. de Melo, I. S. Gonçalves and M. Pillinger, *J. Mater. Chem.*, 2008, **18**, 894; (*c*) D. Yan, J. Lu, M. Wei, D. G. Evans and X. Duan, *J. Phys. Chem. B*, 2009, **113**, 1381; (*d*) G. G. Aloisi, U. Costantino, F. Elisei, L. Latterini, C. Natali and M. Nocchetti, *J. Mater. Chem.*, 2002, **12**, 3316.
8 (*a*) P. P. Kumar, A. G. Kalinichev and R. J. Kirkpatrick, *J. Phys. Chem. B*, 2006, **110**, 3841; (*b*) L. Mohanambe and S. Vasudevan, *J. Phys. Chem. B*, 2005, **109**, 15651; (*c*) H. Li, J. Ma, D. G. Evans, T. Zhou, F. Li and X. Duan, *Chem. Mater.*, 2006, **18**, 4405; (*d*) M.-A. Thyveetil, P. V. Coveney, H. C. Greenwell and J. L. Suter, *J. Am. Chem. Soc.*, 2008, **130**, 4742; (*e*) D. Yan, J. Lu, M. Wei, H. Li, J. Ma, F. Li, D. G. Evans and X. Duan, *J. Phys. Chem. A*, 2008, **112**, 7671; (*f*) D. Yan, J. Lu, M. Wei, J. Ma, D. G. Evans and X. Duan, *Phys. Chem. Chem. Phys.*, 2009, **11**, 9200; (*g*) R. T. Cygan, J. A. Greathouse, H. Heinz and A. G. Kalinichev, *J. Mater. Chem.*, 2009, **19**, 2470; (*h*) J. L. Suter, R. L. Anderson, H. C. Greenwell and P. V. Coveney, *J. Mater. Chem.*, 2009, **19**, 2482; (*i*) R. L. Anderson, H. C. Greenwell, J. L. Suter, P. V. Coveney and M.-A. Thyveetil, *J. Mater. Chem.*, 2009, **19**, 7251; (*j*) H. Zhang, Z. P. Xu, G. Q. Lu and S. C. Smith, *J. Phys. Chem. C*, 2009, **113**, 559; (*k*) P. P. Kumar, A. G. Kalinichev and R. J. Kirkpatrick, *J. Phys. Chem. C*, 2007, **111**, 13517.
9 A. K. Rappé and W. A. Goddard, *J. Phys. Chem.*, 1991, **95**, 3358.
10 J. R. Maple, M.-J. Hwang, T. P. Stockfisch, U. Dinur, M. Waldman, C. S. Ewig and A. T. Hagler, *J. Comput. Chem.*, 1994, **15**, 162.
11 A. E. Reed, L. A. Curtiss and F. Weinhold, *Chem. Rev.*, 1988, **88**, 899.
12 M. J. Frisch, G. W. Trucks, H. B. Schlegel, G. E. Scuseria, M. A. Robb, J. R. Cheeseman, J. A. Montgomery, Jr., T. Vreven, K. N. Kudin, J. C. Burant, J. M. Millam, S. S. Iyengar, J. Tomasi, V. Barone, B. Mennucci, M. Cossi, G. Scalmani, N. Rega, G. A. Petersson, H. Nakatsuji, M. Hada, M. Ehara, K. Toyota, R. Fukuda, J. Hasegawa, M. Ishida, T. Nakajima, Y. Honda, O. Kitao, H. Nakai, M. Klene, X. Li, J. E. Knox, H. P. Hratchian, J. B. Cross, C. Adamo, J. Jaramillo, R. Gomperts, R. E. Stratmann, O. Yazyev, A. J. Austin, R. Cammi, C. Pomelli, J. W. Ochterski, P. Y. Ayala, K. Morokuma, G. A. Voth, P. Salvador, J. J. Dannenberg, V. G. Zakrzewski, S. Dapprich, A. D. Daniels, M. C. Strain, O. Farkas, D. K. Malick, A. D. Rabuck, K. Raghavachari, J. B. Foresman, J. V. Ortiz, Cui, Q. A. G. Baboul, S. Clifford, J. Cioslowski, B. B. Stefanov, G. Liu, A. Liashenko, P. Piskorz, I. Komaromi, R. L. Martin, D. J. Fox, T. Keith, M. A. Al-Laham, C. Y. Peng, A. Nanayakkara, M. Challacombe, P. M. W. Gill, B. Johnson, W. Chen, M. W. Wong, C. Gonzalez, and J. A. Pople, *Gaussian 03: Revision B.04*; Gaussian, Inc.: Pittsburgh, PA, 2003.
13 H. J. C. Berendsen, J. P. M. Postma, W. F. van Gunsteren and J. Hermans, Interaction models for water in relation to protein hydration, in *Intermolecular Forces*, ed. B. Pullman, Riedel, Dordrecht, The Netherlands, 1981, p. 331.

14 (*a*) M. P. Allen, and D. J. Tildesley, *Computer Simulation of Liquids*, Clarendon, Oxford, 1987; (*b*) A. R. Leach, *Molecular Modeling, Principles and Applications*, Pearson Education Ltd, England, 2nd edn, 2001.
15 H. C. Andersen, *J. Chem. Phys.*, 1980, **72**, 2384.
16 H. J. C. Berendsen, J. P. M. Postma, A. van Gunsteren, A. DiNola and J. R. Haak, *J. Chem. Phys.*, 1984, **81**, 3684.
17 *Discover Module, MS Modeling, Version 2.2*, Accelrys Inc., San, Diego, CA, 2003.
18 M. Ogawa and K. Kuroda, *Chem. Rev.*, 1995, **95**, 355.
19 J. Bujdák and N. Iyi, *Chem. Mater.*, 2006, **18**, 2618.
20 B. Valeur, *Molecular Fluorescence: Principles and Applications*, Wiley-VCH Verlag GmbH, 2001.

